materials

MDPI

Article

An Empirical Dilatancy Model for Coarse-Grained Soil under the Influence of Freeze–Thaw Cycles

Yangsheng Ye [1], Degou Cai [1,*], Shuang Tian [2,3], Hongye Yan [1], Xianzhang Ling [2,3], Liang Tang [2,3] and Yike Wu [2,3]

[1] Railway Engineering Research Institute, China Academy of Railway Sciences Corporation Limited, Beijing 100081, China; yysh@rails.cn (Y.Y.); yanhongye_2005@163.com (H.Y.)
[2] School of Civil Engineering, Harbin Institute of Technology, Harbin 150090, China; ts_hit@163.com (S.T.); xianzhang_ling@263.net (X.L.); tangliang@hit.edu.cn (L.T.); wyk_hit@163.com (Y.W.)
[3] Chongqing Research Institute, Harbin Institute of Technology, Chongqing 401135, China
* Correspondence: caidegou@126.com; Tel.: +86-138-102-85950

Abstract: In the era of high-speed trains, it is very important to ensure the safety and stability of rail tracks under adverse conditions including seasonal freezing and thawing. Freeze–thaw cycles (FTCs) affecting the engineering performance of coarse-grained soil (CGS) is one of the major reasons for track deterioration. The reported results of a number of static freeze–thaw triaxial tests on the shear behaviour of CGS are analysed herein. It was observed that confining pressure (σ_3) and FTCs have a significant influence on the shear behaviour of CGS. In this paper, an empirical mathematical model has been proposed to capture the dilatancy of CGS subjected to FTCs during shearing. The empirical constants a, b, and c proposed in the model are a function of σ_3 and FTCs. The results of the model have been compared with the laboratory experiments and are found to be in good agreement.

Keywords: freeze–thaw cycles; coarse-grained soil; dilatancy; empirical equations

Citation: Ye, Y.; Cai, D.; Tian, S.; Yan, H.; Ling, X.; Tang, L.; Wu, Y. An Empirical Dilatancy Model for Coarse-Grained Soil under the Influence of Freeze–Thaw Cycles. *Materials* **2022**, *15*, 3167. https://doi.org/10.3390/ma15093167

Academic Editor: René de Borst

Received: 3 March 2022
Accepted: 25 April 2022
Published: 27 April 2022

1. Introduction

Coarse-grained soil (CGS) has been widely used in the construction of high-speed railways due to its high shear strength and compaction capacity. A thorough understanding of the engineering properties of CGS is imperative in view of safety, stability and maintenance aspects. Dilation of CGS is important to capture the plastic nature of the material during shearing, and the proper understanding of the stress-dilatancy relationship is imperative for developing a constitutive model that correctly represents the plastic strains.

Systematic study of the relationship between dilatancy and friction angle yielded the simple, classical saw tooth model and the corresponding law of plastic flow [1–3]. Based on the principle of minimum energy ratio, Rowe [2] studied the deformation mechanism in CGS by considering a sliding motion between rigid cylindrical and spherical particles, and established the Rowe stress-dilatancy equation in terms of the stress and strain ratios. Furthermore, Wroth and Basset [4] argued that the expansion rate of soil is closely related to its current stress state. Bolton [5] proposed a new relative dilatancy index by investigating the shear capacity and dilatancy characteristics of various types of sandy soil. Houlsby [6] improved the modelled relationship between the dilatancy angle and the critical state line to characterise the influence of relative density on dilatancy. Mitchell and Soga [7] concluded that the stress-expansion relationship in CGS is greatly affected by factors such as soil structure and confining pressure. Despite significant progress having been made so far in the stress–dilatancy relationships of CGS, comprehensive research incorporating the freeze–thaw cycles (FTCs) effect is limited in a fundamental viewpoint.

Past studies have shown that the engineering properties of CGS used for rail foundations in cold regions have been badly damaged by the FTCs, especially stress dilatancy behaviour [8,9]. A reduction in shear strength and dilation was reported for CGS subjected to FTCs [10–12]. This is why the design and maintenance of HSR requires an insightful

understanding of the fundamental stress–strain response of track construction materials under complex thermo-mechanical conditions. Therefore, some efforts have been made to build a reliable stress dilatancy relationship of soils with incorporating the influence of FTCs to make constitutive models more accurately [13–16]. However, stress-dilatancy relationships incorporating the influence of FTCs are mainly limited to fine-grained materials, whereas stress-dilatancy relationships for CGM that capture the influence of FTCs are still in their infancy. Furthermore, the models in the current research models are too complex to use widely.

In this study, an empirical non-linear stress-dilatancy equation has been proposed to capture the dilatancy behaviour of CGS for a wide range of FTCs. In the models, the effects of FTCs and confining pressures (σ_3) are examined, how they would affect the stress dilatancy relationship and are reflected through changes in the constants a, b and c. Finally, important conclusions and future work opportunities have been discussed.

2. Development of an Empirical Model for CGS under Different FTCs

Dilatancy is fundamental to the simulation of the stress-strain characteristics of soil. Based on the dilatancy equation proposed by Rowe [2], the dilatancy ratio (D_R) and the stress ratio (η) of granular materials can be calculated using Equations (1) and (2), respectively [17].

$$D_R = 1 - \frac{d\varepsilon_v}{d\varepsilon_1} \tag{1}$$

$$\eta = \frac{q}{p} \tag{2}$$

where $d\varepsilon_v$ and $d\varepsilon_1$ denote the volumetric strain increment and the axial strain increment, respectively, and q and p denote deviatoric stress and average stress, respectively.

In this study, the dilatancy characteristics of CGS were further analysed by investigating the dependence of the stress ratio on the dilatancy ratio. Considering the nonlinear behaviour of CGS during the shear process, an empirical dilatancy model for CGS considering FTC, given by Equation (3), was established based on the data collected during the triaxial tests to capture the dilatancy behaviour of CGS under FTCs.

$$\frac{q}{p} = a\left[1 - \frac{d\varepsilon_v}{d\varepsilon_1}\right]^2 + b\left[1 - \frac{d\varepsilon_v}{d\varepsilon_1}\right] + c \tag{3}$$

where a, b, and c denote empirical constants that depend on the confining pressure and the number of FTCs. It is noted that albeit there are no clear physical concepts for the above-mentioned parameters, a simple and practical nonlinear dilatancy model has been initially proposed following some previous studies [18–21].

3. Results and Discussion

3.1. Static Freeze–Thaw Triaxial Test

Static freeze–thaw triaxial tests were conducted at Shijiazhuang Tiedao University to elucidate the static properties of CGS under different FTCs and confining pressures (σ_3) from 30–90 kPa in the low-temperature triaxial laboratory [22]. The CGS used under Harbin-Qiqihar high-speed railway line in Northeast China was used as the test soil (see Figure 1). FTCs were varied from 0 to 10 cycles to represent different field conditions. The triaxial test specimen was 100 mm in diameter and 200 mm in height. More details of the materials and testing procedures can be found elsewhere (e.g., Ling et al. [22], Tian et al. [23]). The stress–strain and volume change behaviour during drained tests at varying FTCs and σ_3 are considered here.

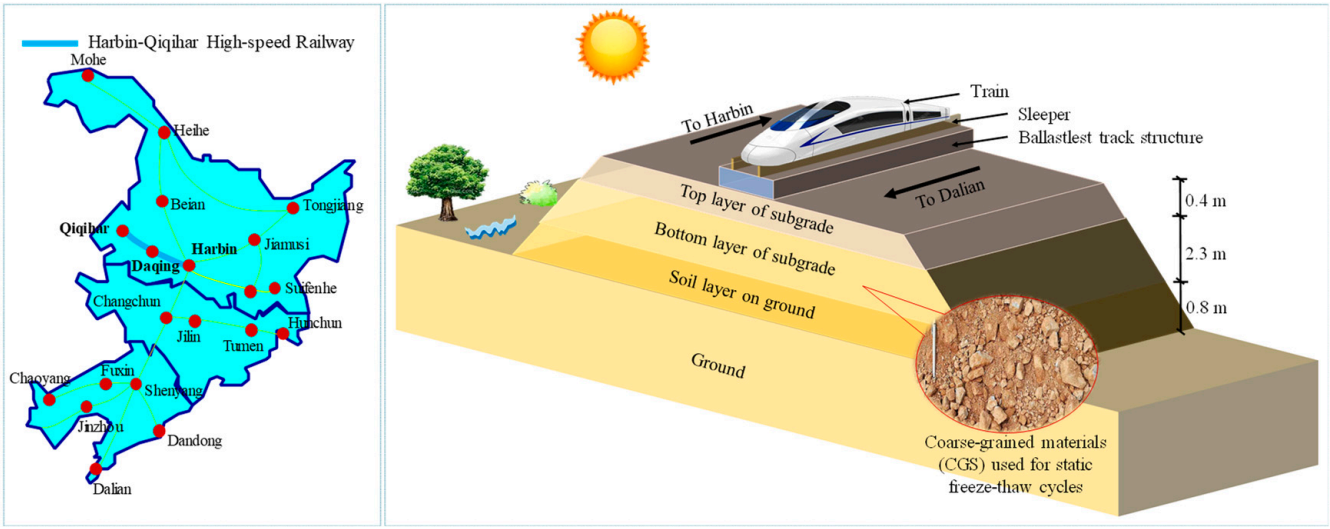

Figure 1. The schematic construction of the Harbin-Qiqihar high-speed railway in Northeast China.

Figure 2 shows the typical variation of deviator stress and volumetric strain with axial strain at different FTCs and σ_3. It is evident that the addition of FTCs has a significant influence on the shear and volumetric strain behaviour of CGS. In general, when σ_3 and FTC increase, the initial compression increases. This is because of an increasing void space after freeze–thaw cycles which allows the specimens to compress. However, the FTCs do not seem to change the overall trends of the stress–strain curves.

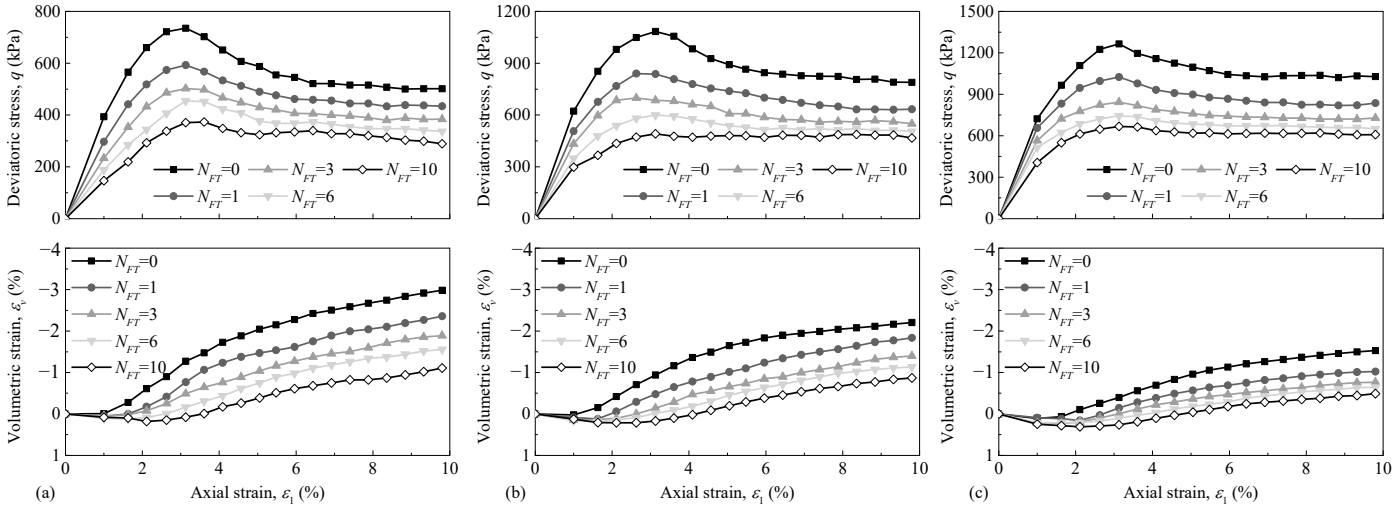

Figure 2. Dependence of deviatoric stress and volumetric strain on axial strain of tested CGS corresponding to different numbers of FTCs (modified after Ling et al. [18]): (**a**) σ_3 = 30 kPa, (**b**) σ_3 = 60 kPa, and (**c**) σ_3 = 90 kPa.

3.2. An Empirical Dilatancy Model for CGS Considering FTCs

The values of *a*, *b*, and *c* under different confining pressures and numbers of FTCs are listed in Table 1. The software used to fit the curve in the current study is Microsoft Excel 2019.

The decrease in stress ratio and dilatancy ratio with the increase in the number of FTCs and confining pressure may be primarily attributed to the following factors. (1) FTCs exert a deteriorating effect on CGS—the modulus and strength of CGS decrease with an increase in the number of FTCs. In addition, after several FTCs, the internal structure of the originally dense CGS changes, and the number of pores between the soil particles are increased, which weakens the dilatancy property of CGS. (2) The mechanical properties of CGS are significantly affected by confining pressure—an increase in confining pressure exerts an inhibitory influence on the dilatancy of CGS.

Table 1. Empirical Constants, *a*, *b*, and *c*.

Confining Pressure, σ_3 (kPa)	FTC, N_{FT} (−)	*a*	*b*	*c*	R^2
30	1	−0.5822	1.8480	1.1303	0.825
	3	−1.3870	3.9102	−0.2301	0.808
	6	−2.4030	6.1883	−1.5292	0.869
	10	−4.5342	11.0304	−4.3194	0.909
60	1	−0.3523	1.3240	1.2973	0.856
	3	−0.6427	1.8171	1.0671	0.543
	6	−2.0180	4.8403	−0.6425	0.823
	10	−3.3690	7.6584	−2.1612	0.845
90	1	−0.2907	1.1040	1.4135	0.539
	3	−0.3732	1.2260	1.3086	0.875
	6	−1.0870	2.6253	0.5784	0.786
	10	−2.4421	5.3794	−0.8606	0.899

As depicted in Figure 3, the stress ratio of CGS increased nonlinearly with an increase in the dilatancy ratio under the influence of FTCs. Under the same confining pressure, the stress ratio of CGS decreased with an increase in the number of FTCs, and the variation range and maximum value of the dilatancy ratio decreased with an increase in the number of FTCs. For the same number of FTCs, the stress ratio of CGS decreased with an increase in confining pressure, and the variation range and maximum value of the dilatancy ratio decreased with an increase in confining pressure.

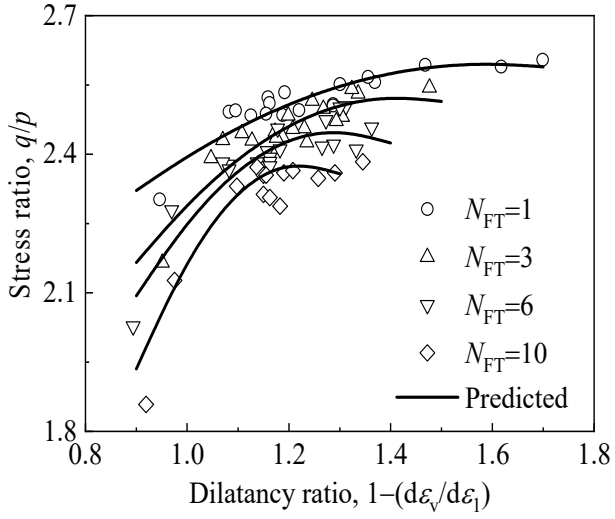

(**a**)

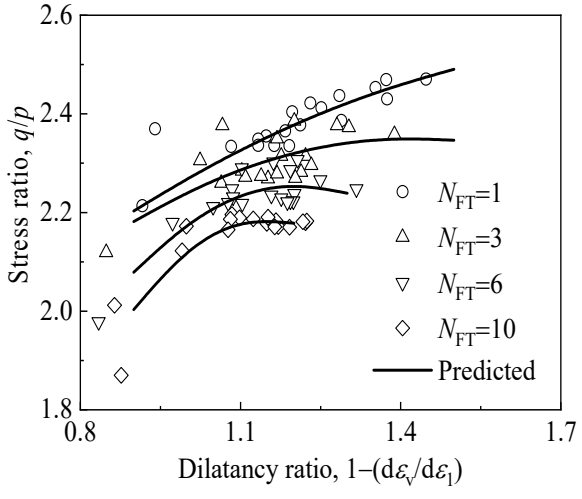

(**b**)

Figure 3. *Cont.*

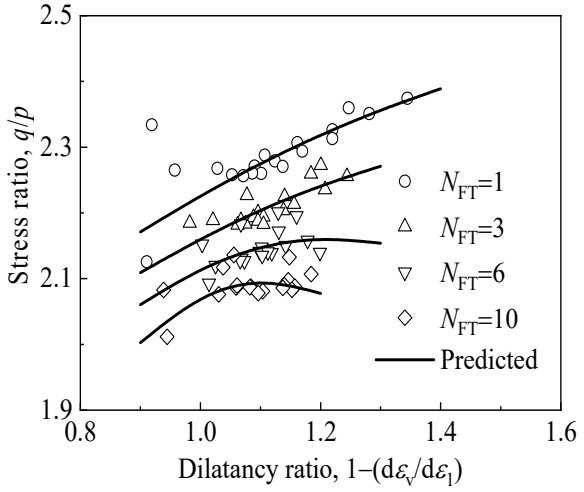

(**c**)

Figure 3. Relationship between the stress ratio and dilatancy ratio of CGS corresponding to different numbers of FTCs and confining pressures: (**a**) σ_3 = 30 kPa, (**b**) σ_3 = 60 kPa, and (**c**) σ_3 = 90 kPa.

As listed in Table 1, the value of the empirical constant, c, under identical confining pressures and different numbers of FTCs, was close to 0 in most cases, either positive or negative. As such data may exhibit significant fluctuations during the subsequent normalisation process, the empirical constant $d = c + 10$ was defined for the subsequent analysis and it was used to represent the variation rule of c. Furthermore, $A \cdot \exp(B \cdot \sigma_3)$ was selected as the normalised factor under different confining pressures. The average empirical constants a, b, and d can be calculated using Equations (4)–(6).

$$a_{avg} = \frac{1}{n}\sum_{i=1}^{n} a_i = \alpha \cdot \exp(\beta \cdot \sigma_3) \quad (4)$$

$$b_{avg} = \frac{1}{n}\sum_{i=1}^{n} b_i = \gamma \cdot \exp(\delta \cdot \sigma_3) \quad (5)$$

$$d_{avg} = \frac{1}{n}\sum_{i=1}^{n} d_i = \zeta \cdot \exp(\eta \cdot \sigma_3) \quad (6)$$

where a_{avg}, b_{avg}, and d_{avg} denote the average empirical constants a, b, and d, respectively; n = 4 corresponds to 1, 3, 6, and 10 FTCs; and α, β, γ, δ, ζ, and η denote undetermined coefficients whose values are presented in Table 2. The values of a_{avg}, b_{avg} and d_{avg} under specific confining pressures can be calculated using Equations (4)–(6).

Table 2. Regression coefficients for model parameters.

Fitting Equations	Regression Coefficients	Values
$a_{avg} = \frac{1}{n}\sum_{i=1}^{n} a_i = \alpha \cdot \exp(\beta \cdot \sigma_3)$	α	−3.2310
	β	−0.0122
$b_{avg} = \frac{1}{n}\sum_{i=1}^{n} b_i = \gamma \cdot \exp(\delta \cdot \sigma_3)$	γ	8.5480
	δ	−0.0132
$d_{avg} = \frac{1}{n}\sum_{i=1}^{n} d_i = \zeta \cdot \exp(\eta \cdot \sigma_3)$	ζ	8.0590
	η	0.0031
$\frac{a_i}{a_{avg}} = M_1 \cdot \exp(N_1 \cdot \mathrm{N_{FT}})$	M_1	0.2898
	N_1	0.2024
$\frac{b_i}{b_{avg}} = M_2 \cdot \exp(N_2 \cdot \mathrm{N_{FT}})$	M_2	0.3517
	N_2	0.1745
$\frac{d_i}{d_{avg}} = M_3 \cdot \exp(N_3 \cdot \mathrm{N_{FT}})$	M_3	1.2390
	N_3	−0.0451

By fitting Equations (7)–(9), the normalised empirical constants a, b, and d corresponding to different numbers of FTCs can be obtained.

$$\frac{a_{\mathrm{i}}}{a_{avg}} = M_1 \cdot \exp(N_1 \cdot \mathrm{N_{FT}}) \tag{7}$$

$$\frac{b_{\mathrm{i}}}{b_{avg}} = M_2 \cdot \exp(N_2 \cdot \mathrm{N_{FT}}) \tag{8}$$

$$\frac{d_{\mathrm{i}}}{d_{avg}} = M_3 \cdot \exp(N_3 \cdot \mathrm{N_{FT}}) \tag{9}$$

where M_1, M_2, M_3, N_1, N_2, and N_3 denote undetermined coefficients whose values are listed in Table 2.

Figure 4 depicts the fitting curves of the average empirical constants, a_{avg}, b_{avg} and d_{avg}, and the normalised empirical constants, a, b, and d. Under different confining pressures, both the normalised empirical constants, a and b, increased nonlinearly and the normalised empirical constant, d, decreased nonlinearly with an increase in the number of FTCs. After 6–10 FTCs, the physical and mechanical properties of CGS tended to stabilise. However, the normalised empirical constants a, b, and d did not stabilise even after 6–10 FTCs. The rate of change of the normalised empirical constants, a and b, increased with an increase in the number of FTCs, while that of the normalised empirical constant, d, remained nearly constant.

As given by Equations (10)–(12), a_n, b_n, and c_n can be obtained by combining Equation (4) and Equation (7), Equation (5) and Equation (8), and Equation (6) and Equation (9), respectively.

$$a_n = \alpha \cdot M_1 \cdot \exp(\beta \cdot \sigma_3 + N_1 \cdot \mathrm{N_{FT}}) \tag{10}$$

$$b_n = \gamma \cdot M_2 \cdot \exp(\delta \cdot \sigma_3 + N_2 \cdot \mathrm{N_{FT}}) \tag{11}$$

$$c_n = \zeta \cdot M_3 \cdot \exp \eta \cdot \sigma_3 + N_3 \cdot \mathrm{N_{FT}} - 10 \tag{12}$$

By substituting Equations (10)–(12) into Equation (3), Equation (13) was obtained, which can be used to predict the relationship between the stress ratio and dilatancy ratio corresponding to any confining pressure and any number of FTCs.

$$\frac{\mathrm{q}}{\mathrm{p}} = \alpha \cdot M_1 \cdot \exp(\beta \cdot \sigma_3 + N_1 \cdot \mathrm{N_{FT}}) \left[1 - \frac{\mathrm{d}\varepsilon_{\mathrm{v}}}{\mathrm{d}\varepsilon_1}\right]^2 + \gamma \cdot M_2 \cdot \exp(\delta \cdot \sigma_3 + N_2 \cdot \mathrm{N_{FT}}) \left[1 - \frac{\mathrm{d}\varepsilon_{\mathrm{v}}}{\mathrm{d}\varepsilon_1}\right] + \zeta \cdot M_3 \cdot \exp(\eta \cdot \sigma_3 + N_3 \cdot \mathrm{N_{FT}}) - 10 \tag{13}$$

3.3. Validation of the Proposed Equation with the Literature

Owing to the lack of sufficient data, the models given by Equations (3) and (13) were verified based on only a small sample of experimental data. To this end, the previously reported triaxial test results of four different types of soil—China's tailing soil [24], Japan's volcanic CGS [25], China's frozen sand [26], and China's CGS for high-speed railway subgrade [22]—were considered. Figure 5 depicts a comparison between the triaxial test results and the predicted curves obtained using the proposed model corresponding to the four types of soil. Table 3 was used to computing the constants a, b, and c for validating the experimental data. The empirical constants a, b and c were found to be −2.892, 4.44, and 0.324, respectively, for tailing soil subjected to 1 FTC, which were used to predict the experimental data reported by Liu et al. [24]. Whereas, a = −4.017, b = 6.409, and c = −0.998 was used to predict the experimental data reported by Ishikawa and Miura [25] for volcanic coarse-grained soil subjected to 1 FTC. Furthermore, the experimental data for sandy soil in frozen state and CGS subjected to 1 FTC reported by He et al. [26] and Ling et al. [22], respectively, were also used to validate the proposed model. The empirical constants a, b and c were found to be −5.514, 11.71, −4.246 and −3.408, 7.797, −2.339, respectively. It is

evident from Figure 5 that the proposed equations (Equations (3) and (13)) have shown a very good agreement with the past experimental data.

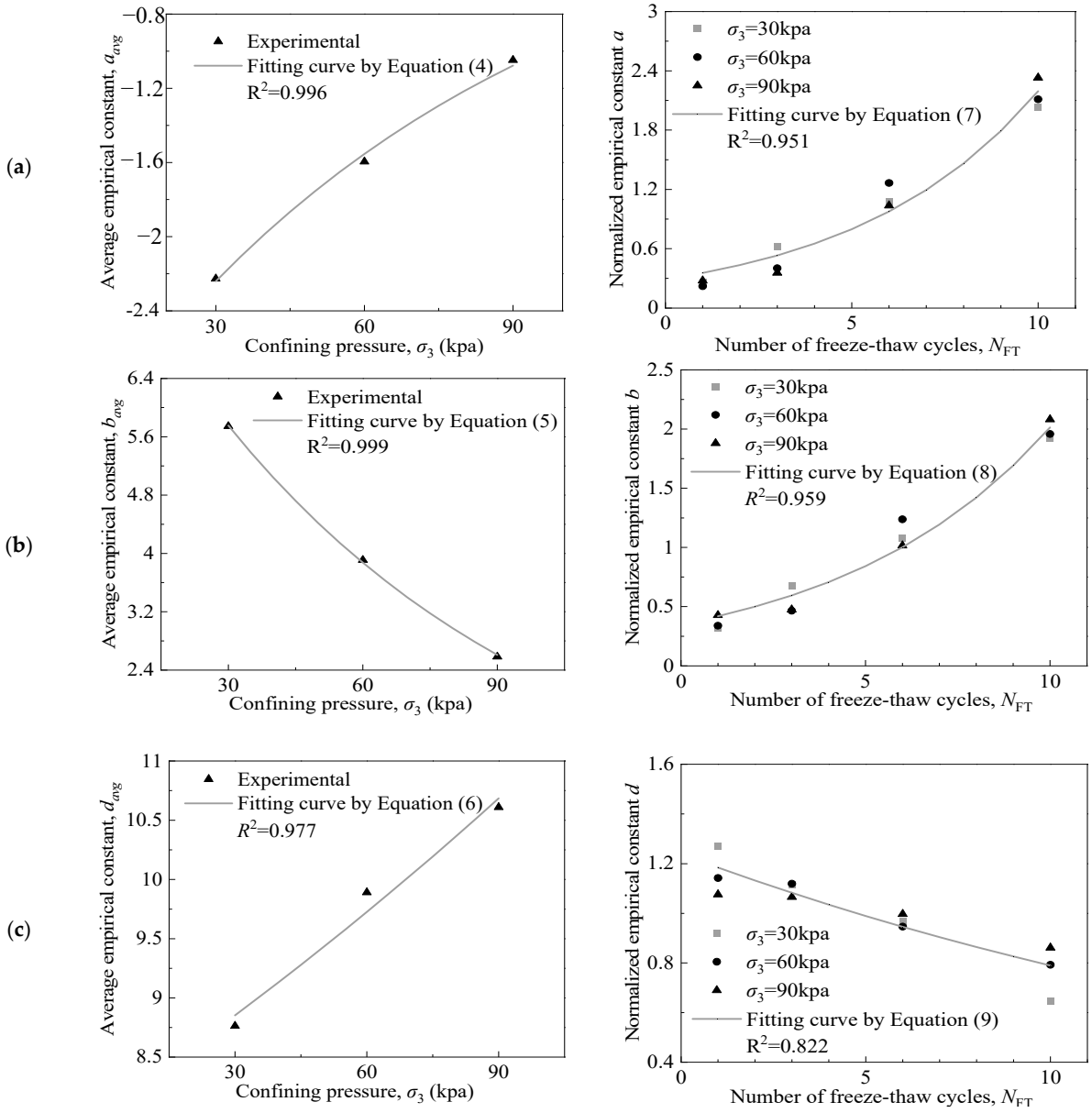

Figure 4. Fitting curves of (**a**) empirical constant *a*; (**b**) empirical constant *b*; and (**c**) empirical constant *d*.

Table 3. Values of the parameters of the prediction model.

Source of Experimental Data	Material	FTC	Confining Pressure, σ_3 (kPa)	a·(a_n)	b·(b_n)	c·(c_n)	R^2
Liu et al. [16]	Tailing soil	N_{FT} = 1	100	−2.892	4.440	0.324	0.816
Ishikawa and Miura [17]	Volcanic coarse-grained soil	N_{FT} = 1	49	−4.017	6.409	−0.998	0.889
He et al. [18]	Sandy soil	Frozen	1000	−5.514	11.710	−4.246	0.633
Ling et al. [14]	Coarse-grained soil	N_{FT} = 1	60	−3.408	7.797	−2.339	0.845

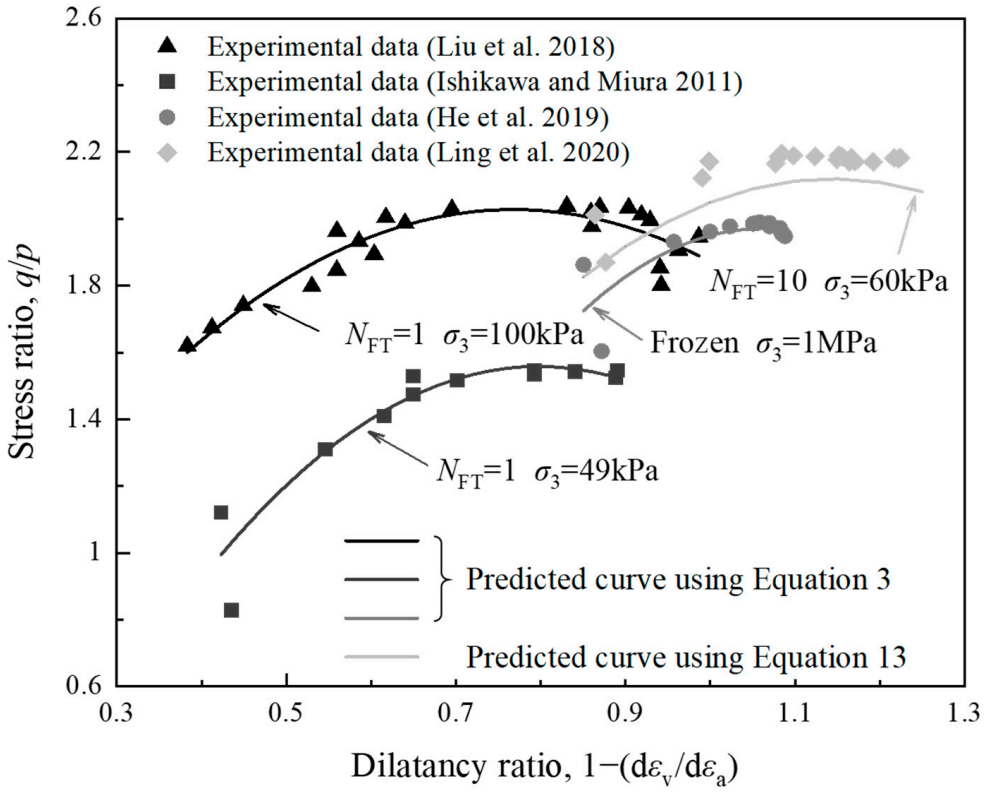

Figure 5. Comparison between predicted and experimental values of stress ratio and dilatancy ratio.

4. Conclusions

Freezing-thawing cycles (FTCs) due to seasonal variations may induce instability in the railway track. Static freeze-thaw triaxial tests on coarse-grained soils (CGS) demonstrated a reduction in the shear strength and dilation upon shearing and further exhibited a non-linear relationship between the stress ratio and dilatancy ratio. Therefore, empirical dilatancy models of CGS were proposed to address the effects of FTCs and confining pressure (σ_3). From the obtained results and analyses presented in this study, the main conclusions are drawn as follows:

(1) An empirical dilatancy model of CGS considering FTCs was proposed to represent the dilatancy of CGS. The relationship between the stress ratio and the dilatancy ratio can be well-captured by a second-order polynomial fitting. The values of the empirical constants a, b and c introduced in this model depend on the FTCs and σ_3.

(2) The best fit a and c values increase in the form of an exponential function with increasing σ_3, while b values exhibit the opposite trend. On the other hand, the changing law of the a and b values increase with increasing FTCs following a form of an exponential function. Meanwhile, c values exhibit the opposite trend. It is interesting to note that the a, b, and c values vary between −0.37 and −4.53, 1.82 and 11.03, −4.32 and 1.41, respectively.

(3) The prediction performance of the proposed model was verified using experimental data, and the validity and applicability of the proposed model was validated. The minimum value of the biggest determination coefficient R^2 is 0.816 except for sandy soil under frozen state, which show that the proposed non-linear stress-dilatancy equation capture the test data well for the FTC conditions.

(4) Further research is needed to address the limitations in the present study; for instance, certain aspects related to stress-induced anisotropy, the effects of creep, long-term cyclic loading and the influence of particle breakage will need to be investigated in the future as an extension of the proposed model.

Author Contributions: Conceptualization, Y.Y. and D.C.; software, S.T.; validation, H.Y. and Y.W.; resources, S.T.; writing—original draft preparation, Y.Y.; writing—review and editing, L.T.; supervision, D.C.; project administration, X.L.; funding acquisition, Y.Y. All authors have read and agreed to the published version of the manuscript.

Funding: This work was supported by the Project Evolution of Service Performance and Hazard Risk Assessment theory of High-speed Railway Foundation under Seasonal Freezing-thawing Environment supported by NSFC (Grant No. 41731288), Project Impacts of Climate Change on Qinghai-Tibet Railway supported by the Systematic major Project of China Railway Group (P2021G047), Project Research on Online Monitoring and Evaluation Technology of Safety State of High-speed Railway-Subgrade System supported by the National Key Research and Development Project of China (Grant no. 2018YFE0207100), and Project Study on Freezing-thawing Mechanism of Water-Gas Migration and Evolution Law of Service Performance of Unsaturated Subgrade of High-speed Railway in Cold Regions supported by Joint Fund of High-speed Railway(U1834206).

Institutional Review Board Statement: Not applicable.

Informed Consent Statement: Not applicable.

Data Availability Statement: Not applicable.

Conflicts of Interest: The authors declare no conflict of interest.

References

1. Taylor, D.W. *Fundamentals of Soil Mechanics*; LWW: Philadelphia, PA, USA, 1948.
2. Rowe, P.W. The stress-dilatancy relation for static equilibrium of an assembly of particles in contact. *Proc. R. Soc. Lond. A Math. Phys. Sci.* **1962**, *269*, 500–527. [CrossRef]
3. Rowe, P.W. The relation between the shear strength of sands in triaxial compression, plane strain and direct. *Géotechnique* **1969**, *19*, 75–86. [CrossRef]
4. Wroth, C.P.; Bassett, R.H. A stress–Strain relationship for the shearing behaviour of a sand. *Géotechnique* **1965**, *15*, 32–56. [CrossRef]
5. Bolton, M.D. The strength and dilatancy of sands. *Géotechnique* **1986**, *36*, 65–78. [CrossRef]
6. Houlsby, G.T. *How the Dilatancy of Soils Affects Their Behaviour*; University of Oxford: Oxford, UK, 1991.
7. Mitchell, J.K.; Soga, K. *Fundamentals of Soil Behavior*; John Wiley & Sons: Hoboken, NJ, USA, 2005.
8. Ling, X.Z.; Zhang, F.; Li, Q.L.; An, L.S.; Wang, J.H. Dynamic shear modulus and damping ratio of frozen compacted sand subjected to freeze–thaw cycle under multi-stage cyclic loading. *Soil Dyn. Earthq. Eng.* **2015**, *76*, 111–121. [CrossRef]
9. Lai, Y.M.; Yang, Y.G.; Chang, X.X.; Li, S.Y. Strength criterion and elastoplastic constitutive model of frozen silt in generalised plastic mechanics. *Int. J. Plast.* **2010**, *26*, 1461–1484. [CrossRef]
10. Liu, Y.; Deng, H.W.; Xu, J.B.; Tian, G.L.; Deng, J.R. Association study on the pore structure and mechanical characteristics of coarse-grained soil under freeze–thaw cycles. *Minerals* **2022**, *12*, 314. [CrossRef]
11. Li, S.Z.; Ye, Y.S.; Tang, L.; Cai, D.G.; Tian, S.; Ling, X.Z. Experimental study on the compaction characteristics and evaluation method of coarse-grained materials for subgrade. *Materials* **2021**, *14*, 6972. [CrossRef]
12. Andrzejuk, W.; Danuta, B.H.; Jacek, G. Physical properties of mineral and recycled aggregates used to mineral-asphalt mixtures. *Materials* **2019**, *12*, 3437. [CrossRef]
13. Huang, S.; Liu, Q.; Cheng, A.; Liu, Y. A statistical damage constitutive model under freeze-thaw and loading for rock and its engineering application. *Cold Reg. Sci. Technol.* **2018**, *145*, 142–150. [CrossRef]
14. Liu, J.; Chang, D.; Yu, Q. Influence of freeze-thaw cycles on mechanical properties of a silty sand. *Eng. Geol.* **2016**, *210*, 23–32. [CrossRef]
15. Liu, Q.; Huang, S.; Kang, Y.; Liu, X. A prediction model for uniaxial compressive strength of deteriorated rocks due to freeze–thaw. *Cold Reg. Sci. Technol.* **2015**, *120*, 96–107. [CrossRef]
16. Tang, L.; Cong, S.; Geng, L.; Ling, X.Z.; Gan, F.D. The effect of freeze-thaw cycling on the mechanical properties of expansive soils. *Cold Reg. Sci. Technol.* **2018**, *145*, 197–207. [CrossRef]
17. Güllü, H.; Khudir, A. Effect of freeze–Thaw cycles on unconfined compressive strength of fine-grained soil treated with jute fiber, steel fiber and lime. *Cold Reg. Sci. Technol.* **2014**, *106–107*, 55–65. [CrossRef]
18. Chu, J. Strain Softening Behaviour of Granular Soils under Strain Path Testing. Ph.D. Thesis, University of New South Wales, Sydney, NSW, Australia, 1991.
19. Chen, X.B.; Zhang, J.S. Effect of clay invasion on shear behavior and dilatancy of unbound aggregate subbase. *Transp. Geotech.* **2016**, *6*, 16–25. [CrossRef]
20. SarojiniAmma, B.K.; Indraratna, B.; Vinod, J.S. A semi-empirical dilatancy model for ballast fouled with plastic fines. *Geomech. Geoeng.* **2018**, *14*, 12–17. [CrossRef]
21. Chen, J.; Indraratna, B.; Vinod, J.S.; Ngo, N.T.; Gao, R.; Liu, Y. Stress-dilatancy behaviour of fouled ballast: Experiments and DEM modelling. *Granul. Matter.* **2021**, *23*, 90. [CrossRef]

22. He, J.; Luo, F.; Zhu, Z.; Zhang, Y.; Ling, C.; Zou, Z. An elastoplastic constitutive model for frozen sandy soil considering particle breakage. *Eur. J. Environ. Civ. Eng.* **2019**, *26*, 320–344. [CrossRef]
23. Ling, X.; Tian, S.; Tang, L.; Li, S. A damage-softening and dilatancy prediction model of coarse-grained materials considering freeze–thaw effects. *Transp. Geotech.* **2020**, *22*, 100307. [CrossRef]
24. Tian, S.; Indraratna, B.; Tang, L.; Qi, Y.; Ling, X. A semi-empirical elasto-plastic constitutive model for coarse-grained materials that incorporates the effects of freeze–thaw cycles. *Transp. Geotech.* **2020**, *24*, 100373. [CrossRef]
25. Ishikawa, T.; Miura, S. Influence of freeze–Thaw action on deformation-strength characteristics and particle crushability of volcanic coarse-grained soils. *Soils Found.* **2011**, *51*, 785–799. [CrossRef]
26. Liu, Y.; Huang, R.; Liu, E.; Hou, F. Mechanical behaviour and constitutive model of tailing soils subjected to freeze-thaw cycles. *Eur. J. Environ. Civ. Eng.* **2021**, *25*, 673–695. [CrossRef]